British Journal of Applied Science & Technology
1(3): 67-93, 2011

SCIENCEDOMAIN *international*
www.sciencedomain.org

Heat Transfer and Friction Factor Correlations for Rectangular Solar Air Heater Duct Having 60° Inclined Continuous Discrete Rib Arrangement

Thakur Sanjay Kumar[1], Vijay Mittal[2*], N. S. Thakur[3] and Anoop Kumar[4]

[1]Department of Mechanical Engineering, G. L. Bajaj Institute of Engineering & Technology, Akbarpur, NH-2, Mathura-Delhi Road, Mathura (UP), India.
[2]Department of Mechanical Engineering, Gateway Institute of Engineering & Technology, Sector 11, Sonipat, (Haryana), India.
[3,4]Department of Mechanical Engineering, N.I.T, Hamirpur (HP), India.

Research Article

Received 24th February 2011
Accepted 6th March 2011
Online Ready 30th March 2011

ABSTRACT

The heat transfer coefficient between the absorber plate and air can be considerably increased by using artificial roughness on the underside of the absorber plate of the solar air heater. An experimental study has been carried out for enhancement of heat transfer coefficient of a solar air heater having roughened air duct provided with artificial roughness in the form 60° inclined discrete rib. Increment in friction factor by provided with such artificial roughness element has also been studied. The effect of system parameters such as relative roughness height (e/D), relative roughness pitch (P/e) and relative gap position (d/W) have been studied on Nusselt number (Nu) and friction factor (f) with relative gap width (g/e) 1 and Reynolds number (Re) varied from 4105 to 20526. Considerably enhancement in heat transfer coefficient has been achieved with such roughness element. Using experimental data correlations for Nusselt number and friction factor have also been developed for such solar air heaters, which gives a good agreement between predicted values and experimental values of Nusselt number and friction factor.

** Corresponding author: E-mail: vmittal1231@rediffmail.com*

Keywords: Solar air heater, artificial roughness, Nusselt number, Friction factor;

NOMENCLATURE

A_o: Cross-section area of orifice, m^2; A_P: Area of absorber plate, m^2; C_d: Coefficient of discharge of orifice; C_P: Specific heat of air at constant pressure, j/kg K; D: Hydraulic diameter of duct, m; e: Rib height; e/D: Relative roughness height; f_s : Friction factor of smooth duct; f: Friction factor of roughened duct; g: Gap width, m; H: Depth of duct, m; h: Convective heat transfer coefficient, w/m^2K; $(\Delta h)_o$ Difference of manometric fluid levels in U-tube manometer, m; $(\Delta h)_d$ Difference of manometric fluid levels in micro manometer, m; K: Thermal conductivity of air, w/mK; L: Length of test section, m; $\dot{m}$: Mass flow rate, kg/s; Nu: Nusselt number of roughened surface; Nu_s: Nusselt number of smooth surface; P: Pitch of rib, m; P/e: Relative roughness pitch; Q_u: Useful heat gain, w; T_f: Mean temperature of air, K; T_i: Inlet temperature of air, K; T_o: Outlet temperature of air, K; T_P: Average temperature of plate, K; β: Ratio of orifice diameter to pipe diameter; η: Efficiency parameter; ρ: Density of air, kg/m^3; ρ_m : Density of manometric fluid, kg/m^3; V: Velocity of air, m/s; W: Width of duct, m; α: Angle of attack, (°)

1. INTRODUCTION

The thermal performance of flat-plate solar air heater is generally poor because of two reasons: low thermal capacity of air and low convective heat transfer coefficient between air and the absorber plate. The low value convective heat transfer coefficient is generally attributed to the presence of a viscous sub layer, which can be broken by providing artificial roughness on the heat-transferring surface. The artificial roughness has been used extensively for the enhancement of forced convective heat transfer, which further requires flow at the heat-transferring surface to be turbulent. However, the artificial roughness results in higher frictional losses leading to excessive power requirement for the fluid to flow through the duct. It is therefore, desirable that the turbulence must be created only very close to the surface i.e., in laminar sub layer only, where the heat exchange take place and the core of the flow is not unduly disturbed to avoid excessive losses. This can be done by keeping the height of the roughness elements small in comparison to the duct dimensions (Gupta et al., 1993). The ribs in the rectangular solar air heater disturb the flows, promote flow mixing and turbulence, break the laminar sub layer, and induced secondary flows, thus increasing the heat transfer rate. A large number of studies for heat transfer enhancement and flow characteristics have been performed for various rib design parameters, such as the shapes of rib cross-sections, rib heights, angles of attack, rib-to-rib pitches, and rib arrangements. Han et al. (1985) investigated the effect of the ratio of rib pitch to height, and rib height to equivalent hydraulic diameter on friction factor and heat transfer coefficient for Reynolds number range of 7,000 to 90,000, relative roughness pitch range of 10 to 40, and relative roughness height range of 0.021 to 0.063. He found that the maximum values of friction factor and the Stanton number occur at a relative roughness pitch of 10. Both the average friction factor and Stanton number increase with increasing relative roughness height. Han et al. (1989) investigated that angled or inclined ribs give higher heat transfer rate than the transverse ribs, and narrow aspect ratio ducts perform better than wide aspect ratio ducts for constant pumping power. The angled ribs give higher heat transfer rate than transverse ribs,

because of the secondary flow induced by the rib angle, in addition to breaking the viscous sub-layer and producing local wall turbulence. Han and Park (1988) investigated the combined effect of the rib angle of attack and the channel aspect ratio on the heat transfer and friction characteristics of developing flow in short rectangular channel with a pair of opposite rib roughened walls for Reynolds number range of 10,000 to 60,000. They reported that the maximum heat transfer and pressure drop is obtained at angle of attack of 60° and a square channel provides a better heat-transfer performance than the rectangular channel.

It is found that the transverse ribs enhance the heat transfer coefficient by about 1.7 times than that of the conventional smooth duct due to the flow separation at ribs and reattachment of flow between two adjacent ribs. Further studies (Han et al., 1978; Gee and Webb, 1980; Sethumadhavan and Rao, 1983) showed that parallel angled ribs provide a better heat transfer performance than transverse ribs because of the secondary flow induced by the rib angle in addition to the breaking of viscous sub-layer and producing local wall turbulence. In order to promote higher levels of flow turbulence, further experiments were performed by displacing the angled ribs according to a crossed arrangement or a V-shaped arrangement with the apex of V pointing upstream or downstream (Han et al., 1991; Kukreja et al., 1993; Gao and Sunden, 2001). Due to development of two vortices cells compared to only one cell formed with inclined ribs. It is interesting to note that the V-shaped ribs performed better when pointing upstream (Han et al., 1991). Gao and Sunden (2001) found that, for a rectangular channel 60˚ V-shaped ribbed on both sides produced higher heat transfer enhancement when pointing downstream of the main flow direction (rather than upstream), seemingly contradicting result of (Han et al., 1991).

The next step, aimed at achieving even more efficient rib displacements from the heat transfer point of view, consisted in interrupting the continuity of ribs, on the ground that broken V-shaped or parallel ribs can create more secondary flow cells and produce more local turbulence than the continuous V-shaped or parallel ribs. Lau et al. (1991) investigated the turbulence heat transfer and friction for a fully developed flow in a square duct with inclined and transverse discrete ribs. The average Stanton number in the 90° discrete rib case is about 10 to 15 percent higher than that in the 90° transverse rib case. For a given pumping power, 60° and 45° discrete ribs enhance the ribbed wall heat transfer about 5 to 19 percent and about 11 to 33 percent more than the corresponding angled full ribs. Parallel 60° discrete ribs have the highest ribbed wall heat transfer and parallel 30° discrete ribs cause the lowest pressure drop. Han and Zhang (1992) investigated the effect of the broken rib orientation on the local heat transfer distribution and pressure drop in a square duct with two opposite roughened walls. The results show that 60° parallel broken ribs or 60° V-shaped broken ribs provide higher heat transfer augmentation than 45° parallel broken or 45° V-shaped broken ribs. It has also been observed that 60° parallel broken ribs or 60° V-shaped broken ribs perform better than 60° parallel continuous ribs or 60° V-shaped continuous ribs. The heat transfer augmentation is about 2.5 to 4 times for the broken rib configuration and about 2 to 3 times for the continuous rib configuration with about 7 to 8 times pressure penalty as compared to smooth duct. Cho et al. (2000) examined the effect of the angle of attack and the number of discrete ribs. The region between the discrete ribs accelerated the flows, and the accelerated flows increased the heat transfer coefficient locally. Cho et al. (2003) investigated the effect of a gap in the inclined ribs on heat transfer in a square duct and reported that a gap in the inclined rib accelerates the flow and enhances the local turbulence, which will result in an increase in the heat transfer. They reported that the inclined rib arrangement with a downstream gap position shows higher enhancement in heat transfer compared to that of the continuous inclined rib arrangement. Cavallero and Tanda (2002) have investigated experimentally forced convection heat transfer in channel with rib

turbulators by means of liquid crystal thermography and revealed that average heat transfer coefficient for the ribbed surfaces is higher than those for the unribbed surface by a factor of up to 2 for continuous ribs, while by a factor of up to 3 for broken ribs. Tanda (2004) investigated heat transfer in rectangular channels with transverse and V-shaped broken ribs with p/e = 8 and found that pairs of high heat transfer coefficient lobes are located aside the line normal to ribs (when transverse) or aside the bisector of ribs (when V-shaped). Most of the investigators carried out so far have applied the artificial roughness on two opposite walls with all four walls being heated. It is noted that for the application of this concept of enhancement of heat transfer incase of solar air heaters, roughness elements have to be considered only on one wall, which is subjected to uniform heat flux while the remaining three walls were insulated. Therefore, the solar air heaters were modeled as a rectangular channel having one rough wall and three smooth walls. This makes the fluid flow and heat transfer characteristics distinctly different from those found in the case of channel with two opposite roughened walls, roughened annular and circular tubes. Further the range of Reynolds number applicable in solar air heaters are of lower range in comparison of the heat exchangers.

Many investigators (Prasad and Saini 1988; Gupta et al., 1993; Verma and Prasad 2000; Karwa et al., 1999; Karwa et al., 2001; Bhagoria et al., 2002; Muluwork et al., 1998; Momin et al., 2002; Karwa 2003; Sahu and Bhagoria 2005; Saini and Verma 2008; Varun et al., 2008) investigated the effect of artificial rib roughness in various forms on the airflow side of the absorber plate to enhance the thermal performance of solar air heaters. Studies carried out by these researchers have shown that the geometry of rib, namely shape, pitch, angle of attack and height, affects significantly the heat transfer and friction characteristics of the duct.

It has been found (Lau et al., 1991; Han and Zhang 1992; Cho et al., 2000; Cho et al., 2003; Cavallero and Tanda, 2002; Tanda, 2004) that discrete inclined or V-shaped rib arrangement can yield better performance as compared to continuous rib arrangement. Moreover, since the use of broken ribs increases both heat-transfer and friction, evaluation criteria have to be developed to demonstrate the performance advantage relative to smooth passages of equal hydraulic diameters. However, investigators have not been carried out so far to optimize the rib position, rib height of the 60°inclined discrete rib and also to locate the optimum position of gap. The present work has been taken up to determine optimum position and height of rib elements as well as optimum location of rib gap, while discretizing the 60° inclined (non-transverse) ribs for enhancing the performance as compared to smooth solar air heater.

In the present work, experimental investigation on the performance of solar air heater ducts, having the absorber plate with artificial roughness in the form of 60° inclined rib, provided with a relative gap width (g/e) = 1, has been carried out. The flow Reynolds number has been varied between 4105 and 20526. The variations of Nusselt number and friction factor as a function of roughness parameters including gap position, roughness pitch and roughness height have been evaluated to compare with smooth plate solar air heater. Using experimental data correlations have been developed for predicting the Nusselt number and friction factor for such solar air heaters.

Table. 1 summarizes the various arrangements of discretizing the inclined ribs employed by these investigators.

Investigators	Roughness parameters	Roughness geometry
Lau et al. [1991]	(P/e) = 10, e/D = 0.625 W/R = 10 α = 90° and 45° Re = 1000 - 30000	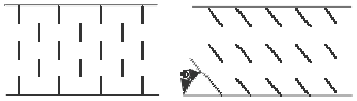
Lau et al. [1991]	(P/e) = 10, e/D = 0.625 W/R = 10 α = 90° and 60° Re = 10000 - 80000	
Hans et al. [1992]	(P/e) = 10, e/D = 0.625 W/R = 10 α = 90°, 60° and 45° Re = 15000 - 60000	
Gao et al. [2009]	(P/e) = 8, e/D = 0.0743 W/R = 2.04 α = 90° and 45° Re = 25000 - 70000	
Gao et al. [2008]	(P/e) = 8, Gap position = W/3 and 2W/3, gap width = width of rib, e/D = 0.8 W/R = 10 α = 60° Re = 25000 - 70000	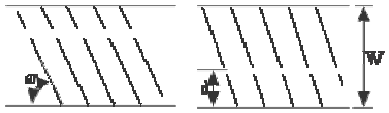

Table 1. Discretizing arrangements of inclined rib

2. ROUGHNESS GEOMETRY AND RANGE OF PARAMETERS

The roughness parameters are determined by rib height (e), rib pitch (p), gap position (d) and gap width (g). These parameters have been expressed in the form of the following dimensionless roughness parameters:

i. Relative roughness pitch (P/e)
ii. Relative roughness height (e/D)
iii. Relative gap position (d/W)
iv. Relative gap position (g/e)

The values of these dimensionless roughness parameters and range of Reynolds number covered in this study are given in Table. 2

The range of Reynolds numbers for the present experimentation is selected on the basis of the mass flow rates reported in the literature for the solar air heater. The range of relative roughness height is selected on the basis of the height of the viscous sub-layer such that the rib breaks the sub-layer and produces the turbulence near the wall region only. The range of relative roughness pitch is selected on the values reported in the literature. The range of relative gap position is selected on the basis of consideration of secondary flow. The relative gap width (g/e) value is selected as 1. Similarly, the value of the angle of attack is chosen as

60˚, to achieve maximum enhancement of heat transfer (Han and Park 1988). The schematic of the geometry of inclined discrete rib used in this experimental is shown in Fig. 1.

Table 2. Dimensionless roughness parameters and range of Reynolds number

Sl. No.	Roughness and flow parameters	Range of parameters
1	Reynolds number (Re)	4105.2-20526.2 (6 values)
2	Relative roughness height (e/D)	0.0249, 0.0374 and 0.0498
3	Relative roughness pitch (P/e)	8, 12 and 16
4	Relative gap position (d/W)	0.15, 0.25 and 0.35
5	Relative gap width (g/e)	1

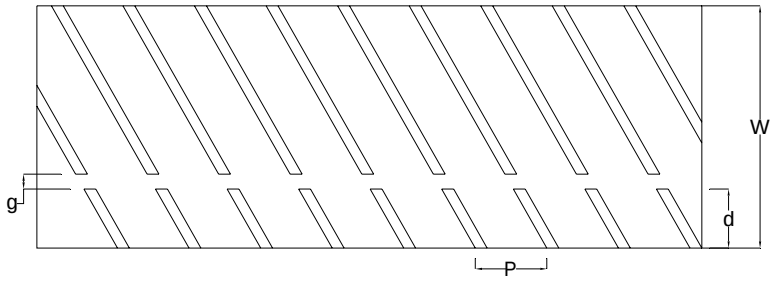

Fig. 1. Geometry of 60˚ inclined discrete rib roughness

3. EXPERIMENTAL PROGRAM

3.1 EXPERIMENTAL APPARATUS

The experimental setup is an open loop flow system has been designed and fabricated to conduct experimental investigation on the heat transfer and fluid flow characteristics of a rectangular duct having 60˚ inclined discrete ribs roughness on the heated surface. The experimental data collected are to be used to develop correlations for heat transfer coefficient and friction factor. Fig. 2 is a schematic diagram of the indoor experimental setup including test section. The experimental setup consists of a test duct along with entrance and exit sections, a blower and control valves, a calibrated orifice plate and various devices for measurement of pressure and temperature drop. The blower sucks atmospheric air through the duct, having artificial roughness produced by fixing 60˚ inclined discrete ribs on the underside of the top plate. The flow through the duct can be controlled by means of control valves provided on the line. Mass flow rate of air was measured by means of an orifice meter on the suction side and connected to an inclined manometer. The wooden rectangular duct has internal size as 2200 mm × 158 mm × 23 mm depicting an aspect ratio of 6.9 as shown in Fig. 3. It is constructed from wood. The test section has a length of 1000 mm with a cross section of 158 mm × 23 mm. It consists of an entrance section, a test section and an exit section having lengths as 550 mm, 1000mm and 650 mm respectively. It may be noted that for turbulent flow regime, ASHRAE Standard 93-77 (1950) recommends entry and exit

lengths as 5 $\sqrt{W \times H}$ and 2.5 $\sqrt{W \times H}$ respectively, which has been used in designing the duct for this experimental work. In the exit section three equally spaced baffles are provided after the test section at each 75 mm lengths for the purpose of mixing the delivered air. At the end of duct a plenum was provided to connect the rectangular duct with circular pipe. An aluminum plate 1000 mm x 158 mm x 8 mm is used as artificially roughened plate at the test section of the duct. The artificial roughness was produced by pasting the aluminum wires on to the underside. The diameter of wire has been varied to get different heights of roughness. This plate is heated from the top by means of an electric heater assembly and is subjected to uniform heat flux. An electric heater having a size of 1000 mm x 158 mm was fabricated by combining series and parallel loops of resistance heating wire fitted on 5 mm asbestos sheet. The back side of the heater was insulated with glass wool, to minimize thermal energy losses. The heater placed 42 mm above the roughened absorber plate with the help of wooden spacers. A mica sheet of 0.5 mm thickness is provided between the electric heater and the roughened aluminum plate to avoid the direct contact between heater coil and absorber plate. Energy input to the heater was controlled by a variac so that desired levels of heat flux values could be attained. Ambient air was sucked through the duct system by means of a centrifugal blower driven by a 3-phase, 5 HP, 230 V and 2880 rpm motor. The blower is used to suck the ambient air through the rectangular duct using pipelines and delivered to atmosphere. The air flow rate is regulated at desired rate by providing two control valves, one on the inlet side and other on the outlet side of blower. The mass flow rate of air through duct is measured by orifice meter, which is calibrated for flow rate measurement by experimentally measuring orifice meter co-efficient (C_d) as proposed by Scott et al. (2002) and an average value of C_d can be taken as 0.61.

Copper –constantan thermocouples were used for air and absorber plate temperature measurements as shown in Fig. 4. Before installing the thermocouples in place, they were calibrated under similar environmental conditions. Fifteen have been fixed using fast drying epoxy resin, through 2 mm deep hole of 1.5 mm diameter at the back of the plate. After the mixing section, three thermocouples arranged transverse of the duct to measure the exit air temperature. All thermocouples were connected to digital voltmeter through a selector switch so that the output could be measured in milivolt. The bulk temperature of the entrance section is measured by providing one thermocouples at the entrance section. The pressure drop across the test section of the duct was measured by means of a micro-manometer having a least count of 0.01 mm. The micro manometer consists of a movable reservoir, a fixed reservoir and an inclined transparent tube connected to these reservoirs. An air bubble is trapped by means of a hypodermic needle. The movable reservoir is mounted on a sliding arrangement using a lead screw having a pitch of 1.0 mm and a graduated dial having 100 divisions; each division showing a movement of 0.01 mm of the reservoir. The movable reservoir is displaced up or down to maintain the air bubble at the specified location for any pressure difference between the two reservoirs and the movement of the moving reservoir is noted as the pressure difference across the two pressure tapings connected to the reservoirs.

3.2 EXPERIMENTAL PROCEDURE

Before starting any experiments, all the thermocouples were checked carefully so as to indicate the room temperature and all the pressure tapings were checked for air leakage, if any. The micro manometer and the inclined U – tube manometer were properly leveled. After proper checking of instruments, the test setup was checked and readied for conducting experiments. The power supply to the centrifugal blower and the electric heater was switched on and the desired flow rate was set with the help of control valves.

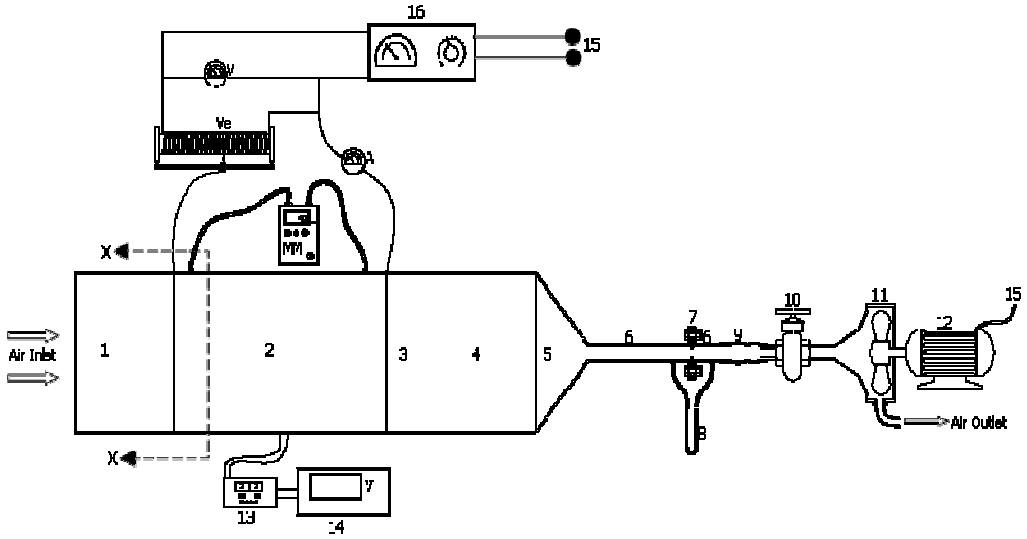

1. Inlet Section
2. Test section
3. Mixing Section
4. Out Let Section
5. Transition Section
6. G. I. Pipe
7. Orifice meter
8. Manometer
9. Flexible Pipe
10. Control Valve
11. Blower
12. Electric Motor
13. Selector – Switch
14. Volt meter
15. Power Source
16. Voltage Stabilizer

MM = Micro-manometer
V = Volt Meter
A = Ammeter
Ve = Variac

Fig. 2. Schematic diagram of experimental set-up

The steady state condition is assumed to have been reached when the temperature at any point does not change for 10 minutes. When a change in the operating conditions is made, it takes about 30 minutes to reach the steady state again. Six values of flow rates were employed for each set of test using constant value of heat flux during the test. After each change of flow rate, the system is allowed to attain the steady state before the data were recorded.

The following parameters were recorded.

i. Pressure difference across the orifice meter.
ii. Pressure drop across the test section.
iii. Temperature of the absorber plate.
iv. Temperature of air at inlet and outlet of the test section.

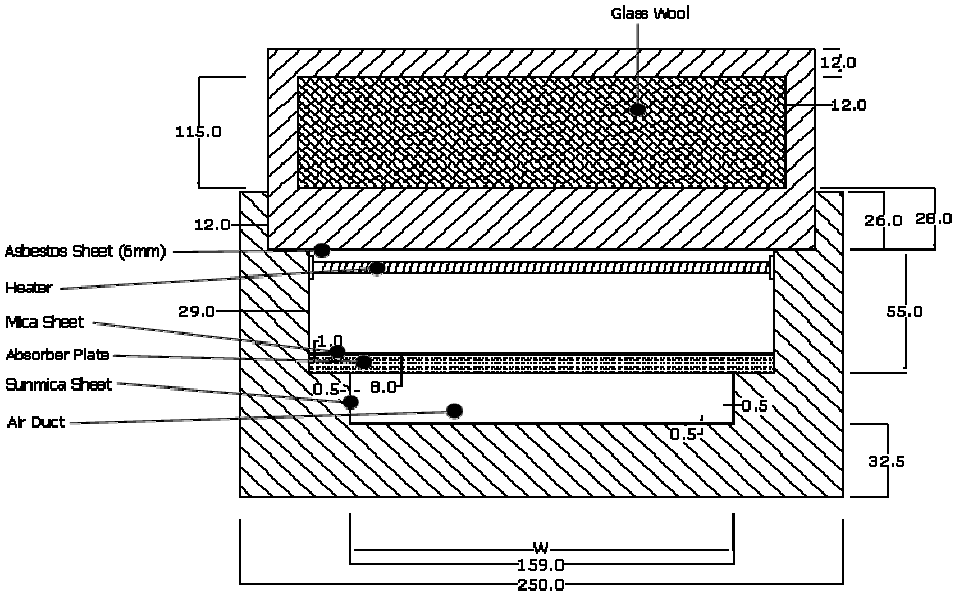

Fig. 3. Cross sectional details of test section

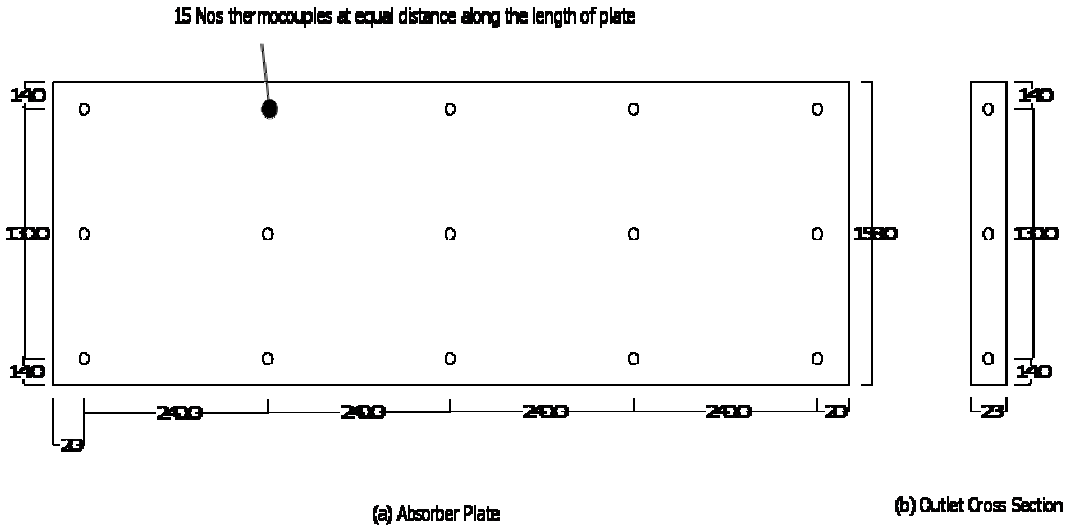

Fig. 4 Location of thermocouples on absorber plate and outlet section of the duct

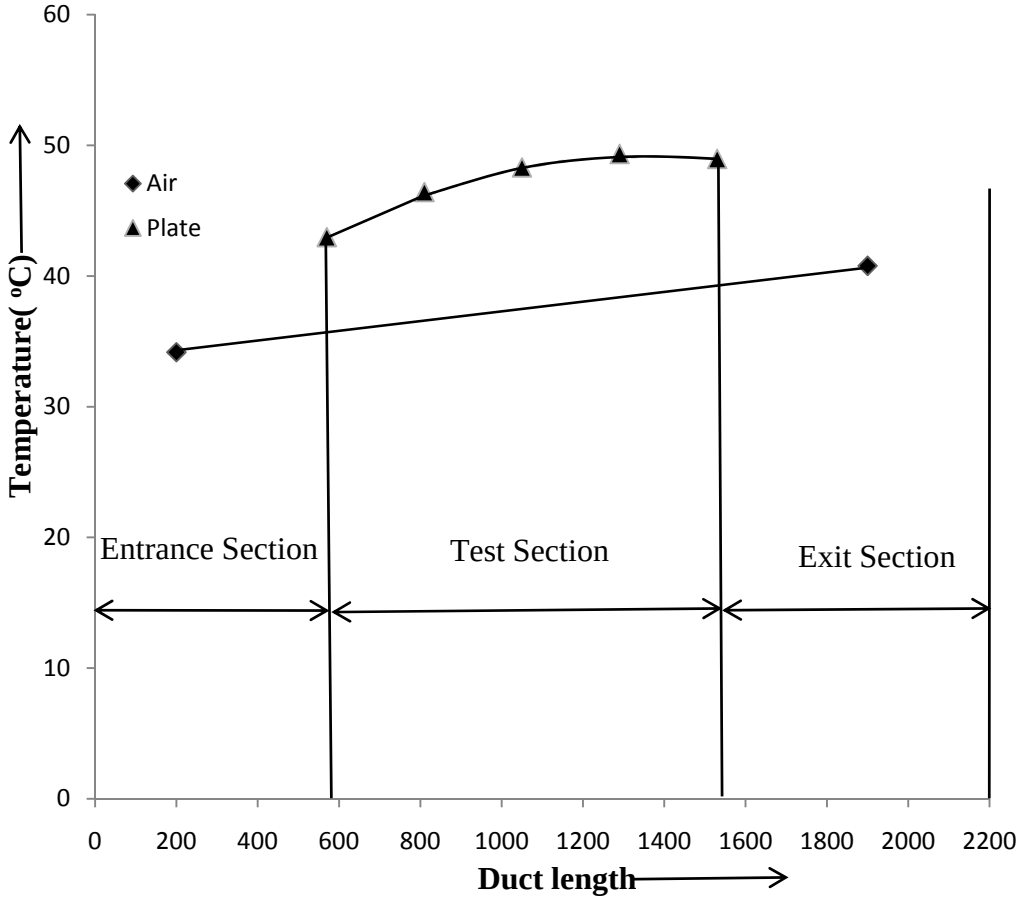

Fig. 5 Plate and air temperature profile along the duct length

4. DATA REDUCTION

Steady state values of the plate and air temperatures in the duct at various locations were used to determine the values of useful parameters, namely mass flow rate"$\dot{m}$", heat supplied to the air"Q_u" and heat transfer coefficient "h " calculated as

$$\dot{m} = C_d \times A_o \times \left[\frac{2.\rho.(\Delta P)_o}{1-\beta^4} \right]^{0.5} \quad (1)$$

Where $(\Delta P)_o = 9.81 \times (\Delta h)_o \times \rho_m \times \sin\theta$

$$Q_u = \dot{m} C_P (T_o - T_i) \quad (2)$$

$$h = \frac{Q_u}{A_P (T_p - T_f)} \quad (3)$$

Where the temperature T_p and T_f are average temperature values of absorber plate and fluis respectively. The average value of plate temperature (T_p) was determined from the detailed temperature profile of the absorber plate indicated by 15 thermocouples at various locations. The typical variation of the plate and air temperatures along the length of the duct is shown in Fig. 5. The convective heat transfer coefficient was then used to obtain Nusselt number, Nu , as

$$Nu = \frac{hD}{K} \tag{4}$$

The friction factor was determined from the measured values of pressure drop, $(\Delta P)_d$, across the test section length, between the two points located 1m apart.

$$f = \frac{2.(\Delta P)_d.D}{4.\rho.L.V^2} \tag{5}$$

Where, $(\Delta P)_d = 9.81 \times (\Delta h)_d \times \rho_m$

It may be noted that prior to actual data collected , the test setup was checked by conducting experiments for a smooth duct. The Nusselt number and friction factor determined from these experimental data were compared with the values obtained from the correlations i.e. Dittus-Blasius equation for friction factor (Bhatti and Shah 1987) and Dittus-Boelter equation for Nusselt number (Kays 1966) in case of smooth duct. These equations are given below:

Blasius equation:

$$f_s = 0.085 \times \mathrm{Re}^{-0.25} \tag{6}$$

Dittus-Boelter equation:

$$Nu_s = 0.024 \times \mathrm{Re} \times \mathrm{Pr}^{0.4} \tag{7}$$

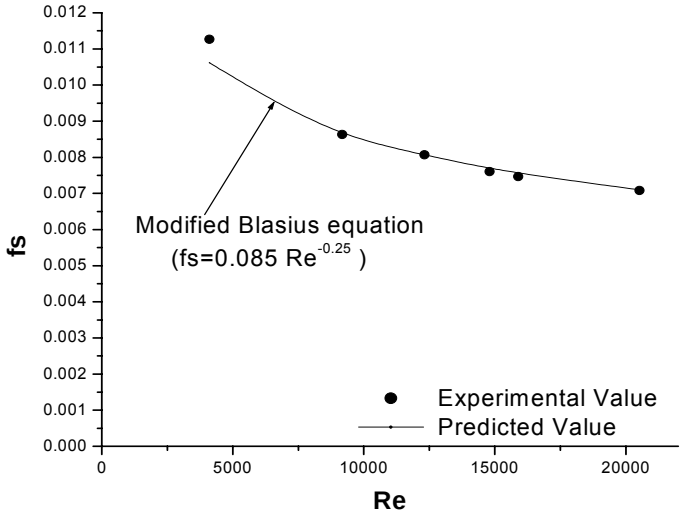

Fig. 6. Friction factor vs. Reynolds number for smooth duct

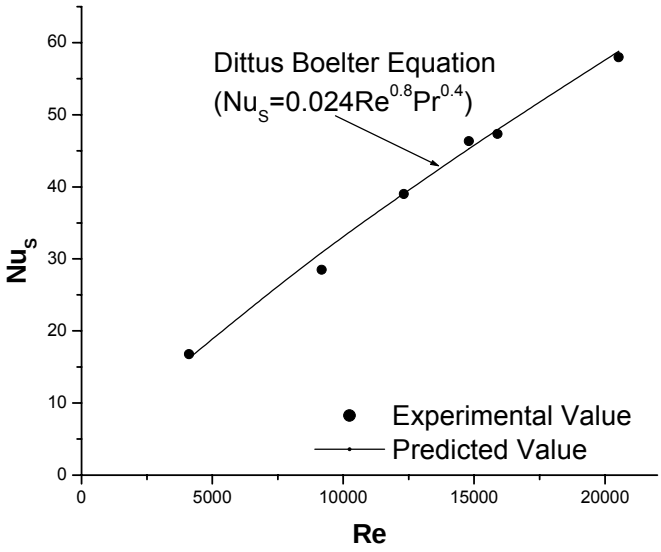

Fig. 7. Nusselt number vs. Reynolds number for smooth duct

The comparison of measured and predicted values of friction factor and Nusselt number are shown in Fig. 6 and Fig. 7, respectively. The agreement is seen to be reasonably good. The above comparison ensures the accuracy of experimental results proposed to be obtained from the present experimental set up and instrumentation.

5. RESULTS AND DISCUSSION

The effect of various flow and roughness parameters on the heat transfer and friction characteristic for flow of air in the rectangular duct are presented below. Results have also been compared with those of the smooth duct under similar flow and thermal boundary conditions to determine the enhancement in the heat transfer coefficient and friction factor.

Fig. 8 shows the variation of Nusselt number for 60º inclined discrete ribbed and smooth duct with Reynolds number and relative roughness pitch for given values of relative gap position and relative roughness height. The values of Nusselt number are found to increase with increasing Reynolds number in all cases as expected. The 60º inclined discrete ribbed ducts can be seen to yield higher Nusselt number as compared to that of the smooth duct as is evident from the comparison of such plots with that of smooth duct.

The data of Fig. 8 has been replotted in Fig. 9 to bring out the effect of relative roughness pitch wherein it can be seen that the Nusselt number increases with increase of relative roughness pitch, attaining maximum value at relative roughness pitch of 12 and then decreases with further increase in relative roughness pitch. It is observed from the plot that the variation of Nusselt number with relative roughness pitch is insignificant at lower values of Reynolds number but at higher Reynolds number, the variation is substantial.

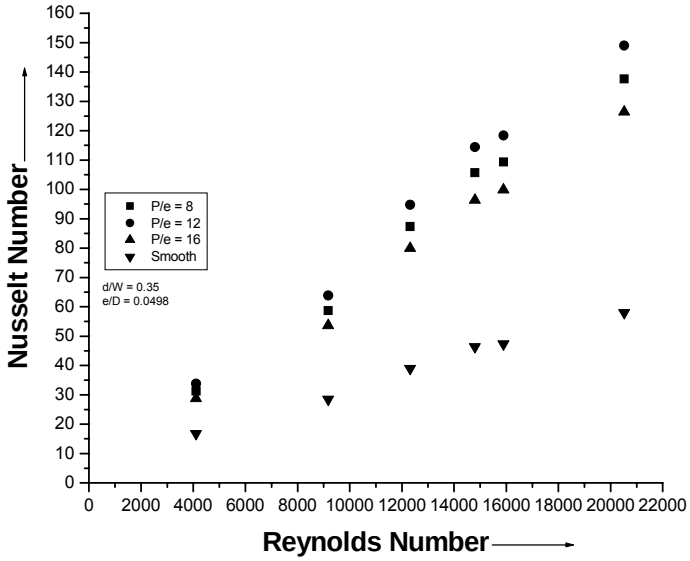

Fig. 8. Nusselt number Vs Reynolds number for e/D= 0.0498 and d/W=0.35

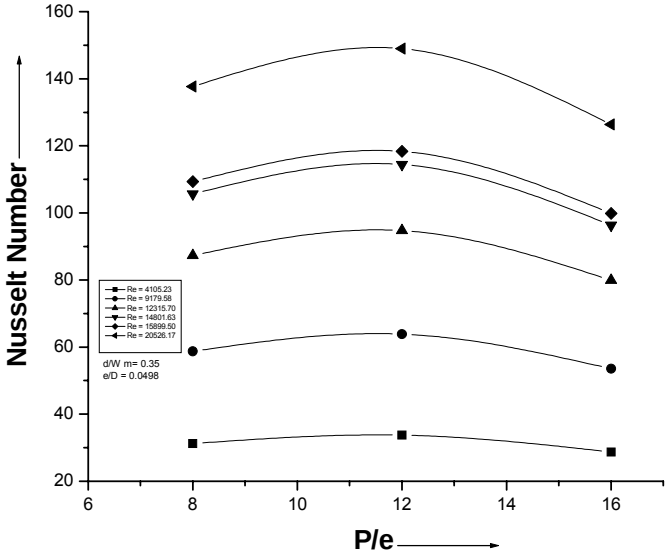

Fig. 9. Nusselt number Vs relative roughness pitch for e/D= 0.0498 and d/W=0.35

Fig. 10 shows the effect of the gap position on Nusselt number for 60º inclined discrete ribbed. It can be seen that the Nusselt number increases with increase in relative gap position (d/W) attaining maximum value at relative gap position of 0.35, the effect being more pronounced at higher values of Reynolds number. Although the plots have been shown for a fixed relative roughness pitch of 12, the trend is general and the same trend is seen at all relative roughness pitch values.

The introduction of a gap in the inclined ribs allows release of secondary flow and main flow through the gap. The main flow is a developed flow with thicker boundary layer, and due to the presence of viscous sublayer, it leads to a low amount of heat transfer. In fact, the ribs are introduced to break this retard flow and let it reattach again with the surface to enhance the heat transfer (Prasad and Saini, 1988). However, in case of gap in the inclined rib, the secondary flow along with the rib joins the main flow to accelerate it, as shown in Fig. 11, which energizes the retarded boundary layer flow along the surface. This increases the heat transfer through the gap width area behind the rib.

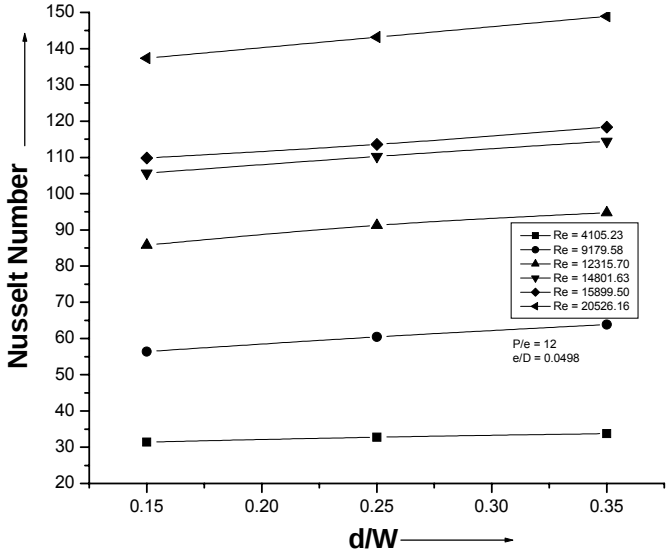

Fig. 10. Nusselt number Vs relative gap position for P/e= 12 and e/D=0.0498

Fig. 12 shows the plots of Nusselt number as a function of relative roughness height (e/D), for 60º inclined discrete ribbed for given values of other roughness geometries parameters. Plots show a monotonic rise in the value of Nusselt number with an increase in the relative roughness height. The 60º inclined discrete ribbed with relative roughness of 12 and gap position to width ratio (d/W) of 0.35 provides the maximum values of the Nusselt number in the order of 2.57 times of the smooth duct.

Fig. 13 shows the effect of Reynolds number and relative roughness pitch on friction factor in the range of Reynolds number investigated for fixed value of other parameters. It is seen that the value of friction factor decreases with increasing Reynolds number in all cases as expected due to the suppression of viscous sub-layer with increase in Reynolds number. The 60º inclined discrete ribbed ducts can be seen to yield higher friction factor as compared to that of the smooth duct. It is observed that for a relative roughness pitch of 12 has maximum friction factor and that of 8.0 has minimum value. The data of Fig. 13 has been replotted in Fig. 14 wherein it can be seen that the friction factor increases with increase in relative roughness pitch, attaining maximum value at relative roughness pitch of 12 and a further increase of relative roughness pitch results in the decrease of friction factor.

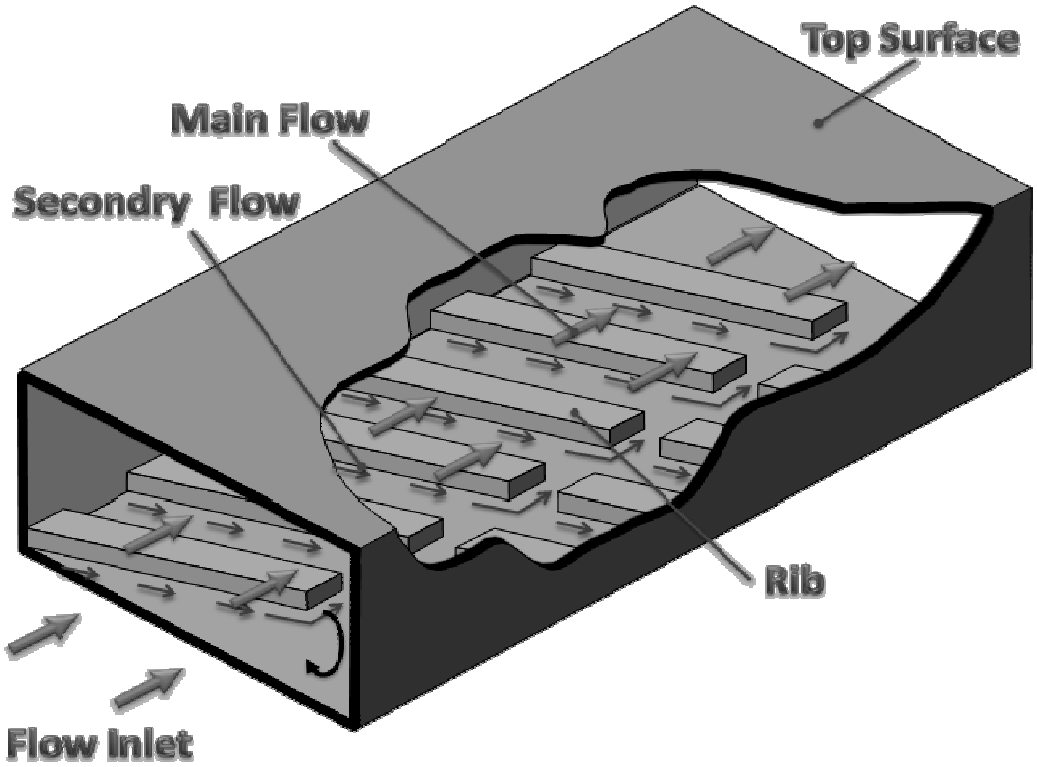

Fig. 11. Flow pattern of secondary flow for inclined discrete rib

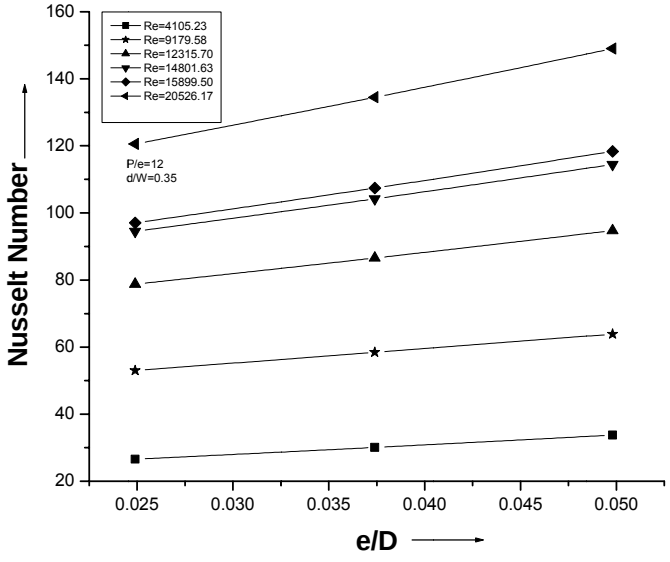

Fig. 12. Nusselt number Vs relative roughness height for P/e= 12 and d/W=0.35

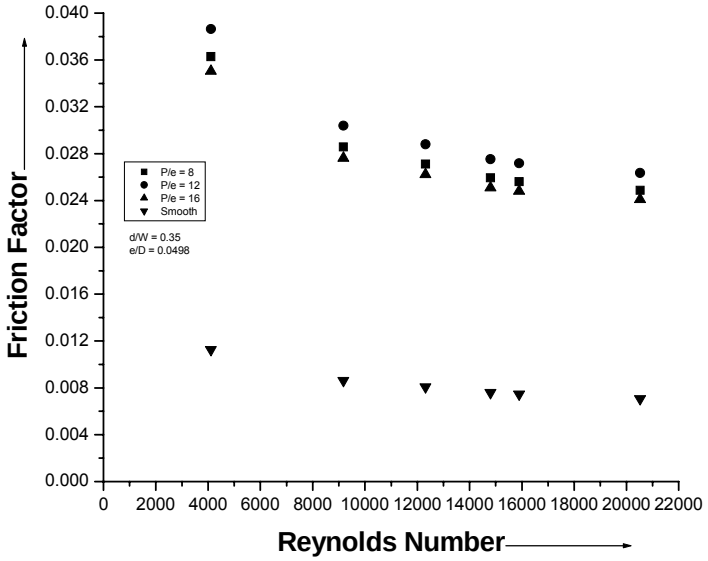

Fig. 13. Friction factor Vs Reynolds number for e/D= 0.0498 and d/W=0.35

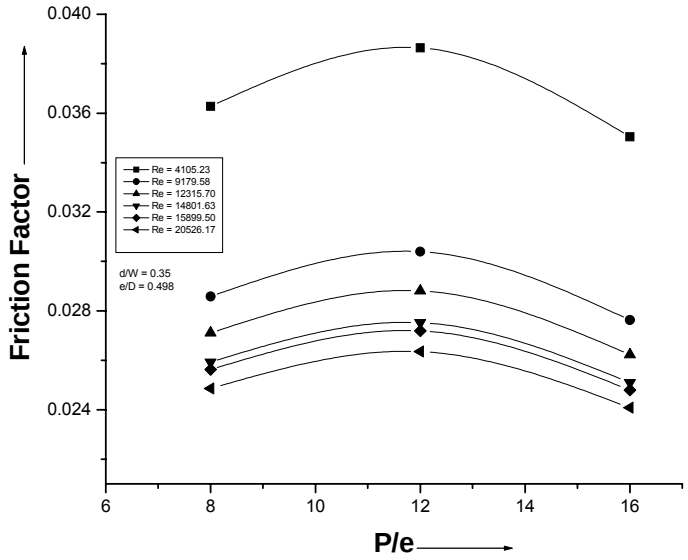

Fig. 14. Friction factor Vs relative roughness pitch for e/D= 0.0498 and d/W=0.35

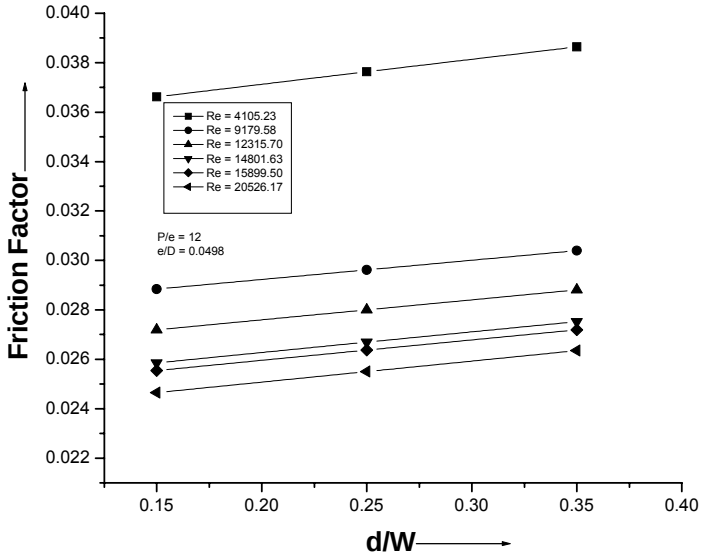

Fig. 15. Friction factor Vs relative gap position for e/D= 0.0498 and P/e=12

Fig. 15 shows the effect of gap position on friction factor in the range of Reynolds number investigated and for fixed values of other parameters. It shows that the value of friction increases with increase in relative gap position. Fig. 16 shows the effect of relative roughness height on the friction factor for fixed value of other roughness and flow parameters. It reveals that there is a monotonic rise in the value of friction factor with the increase in the relative roughness height for a given value of Reynolds number.

The investigation shows that 60º inclined discrete ribbed duct with relative roughness pitch (P/e) of 12, relative gap position (d/W) of 0.35 and relative roughness height (e/D) of 0.0498 yields the maximum value of friction factor in the order of 3.72 times that of smooth duct.

6. CORRELATION FOR NUSSELT NUMBER

The statistical correlations are developed here to cover total 162 experimental data corresponding to all the twenty seven roughened absorber plates. Regression analysis is carried out to find a relationship that yields a best fit equation for Nusselt number. Fig. 17 shows the Nusselt number as a function of Reynolds number. A regression analysis to fit a straight line on graph through the data points yields the following power law relationship between Nusselt number and Reynolds number.

$$Nu = Ao\,\mathrm{Re}^{0.947} \tag{8}$$

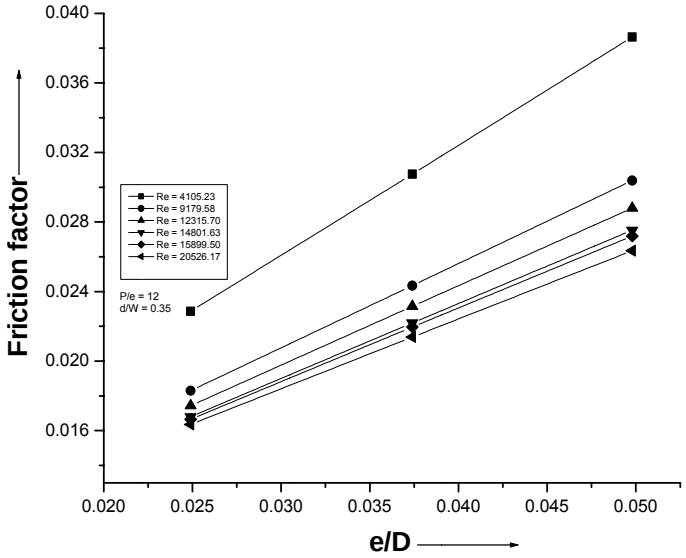

Fig. 16. Friction factor Vs relative roughness height for P/e= 12 and d/W=0.35

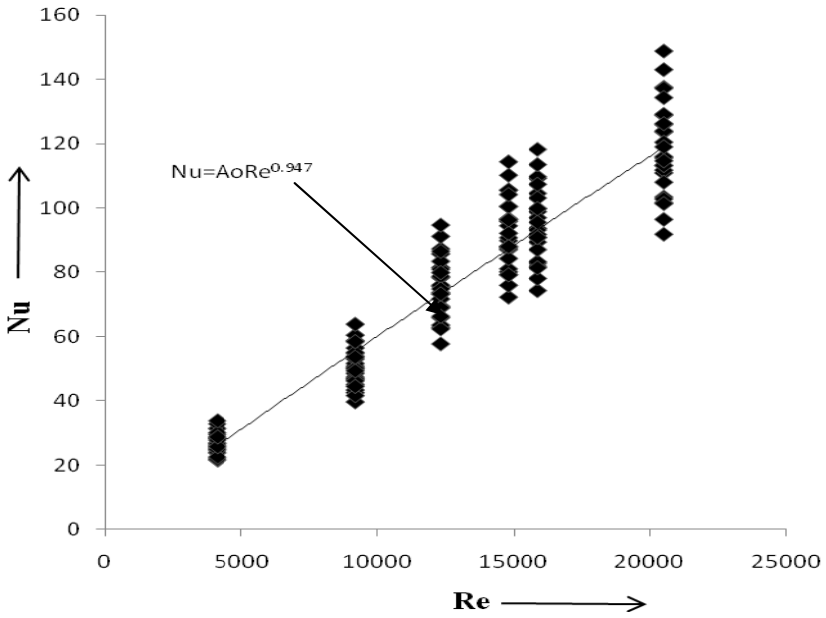

Fig. 17. Nusselt number Vs Reynolds number

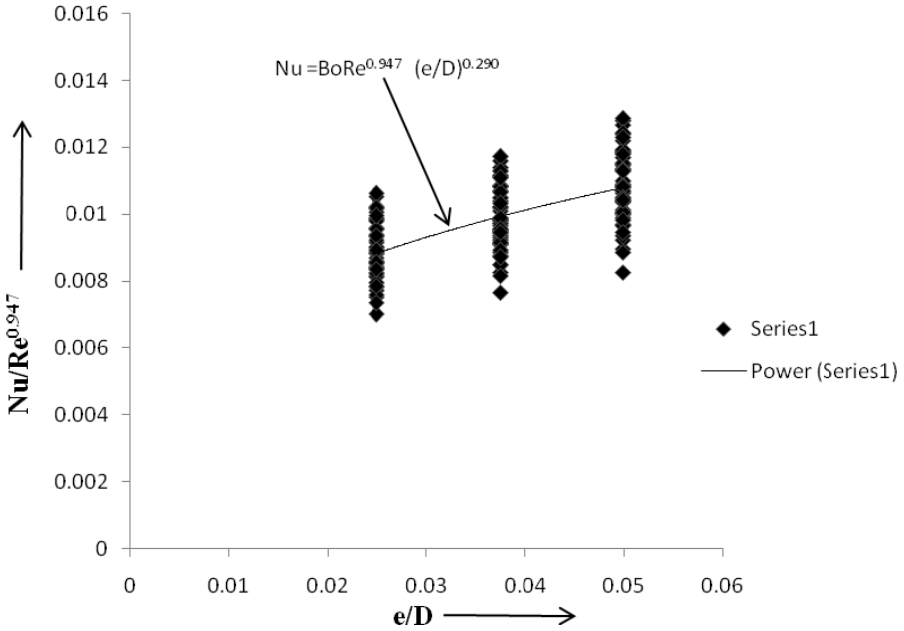

Fig.18. $Nu/(\mathrm{Re})^{0.947}$ **Vs e/D**

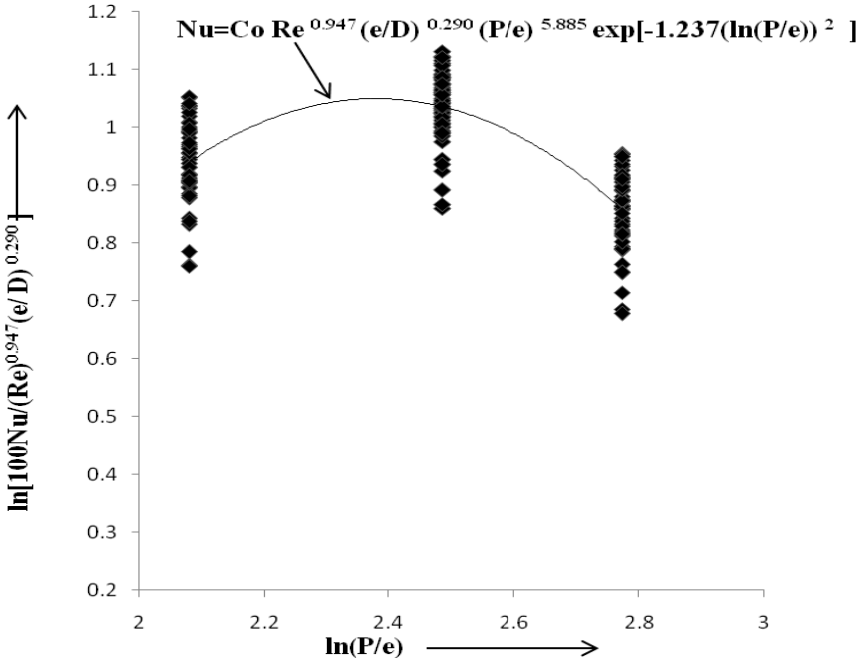

Fig. 19. $\ln\left[\dfrac{100Nu}{(\mathrm{Re})^{0.947}(e/D)^{0.290}}\right]$ **Vs ln(P/e)**

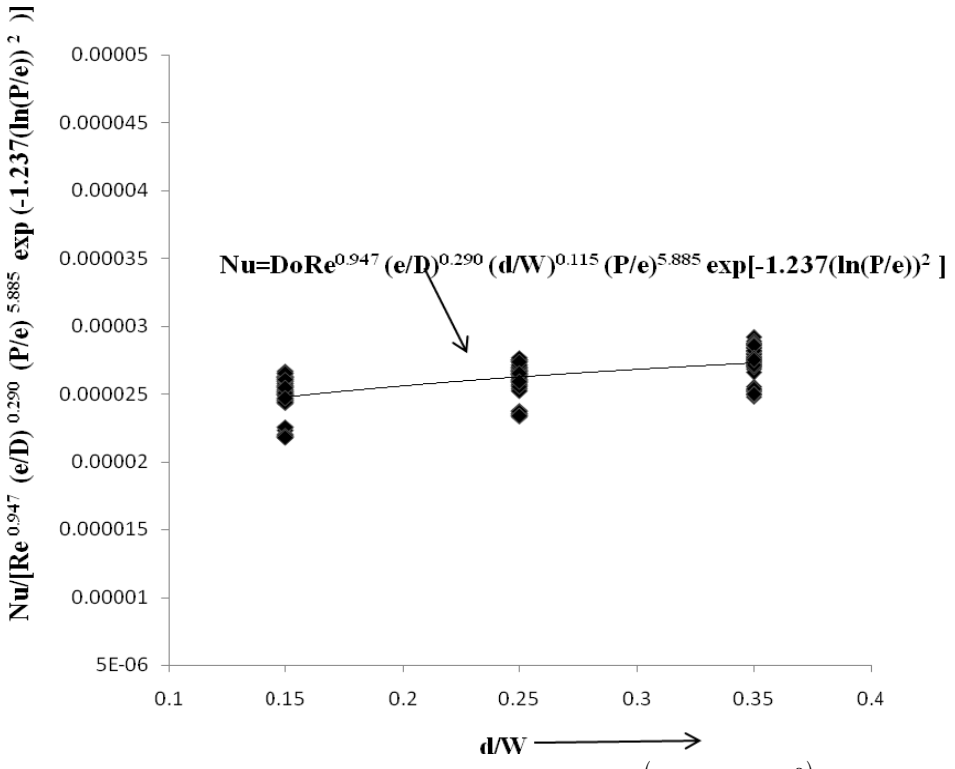

Fig. 20. $Nu/(\mathrm{Re})^{0.947}(e/D)^{0.290}(P/e)^{5.885}\times\exp^{(-1.237\,(\ln(P/e))^2)}$ **Vs d/W**

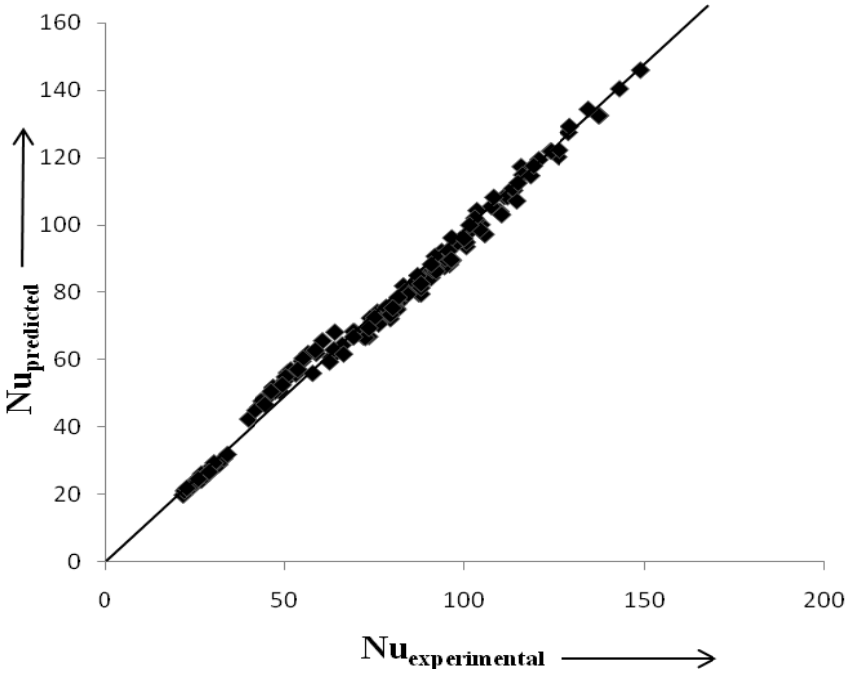

Fig. 21. Comparison of Nusselt number for experimental values with predicted values

The coefficient Ao will in fact be a function of other influencing parameters. Now taking the parameter of relative roughness height of rib (i.e. e/D) in to consideration, the value of $Nu/(\mathrm{Re})^{0.947} = Ao$ corresponding to all values of relative roughness height (e/D) are plotted against relative roughness height, as shown in Fig. 18. The regression analysis to fit a straight line on graph through points yields:

$$\frac{Nu}{(\mathrm{Re})^{0.947}} = Bo\left(e/D\right)^{0.290} \tag{9}$$

Such a relationship was indicated by plots of Nusselt number as a function of relative roughness height of rib (e/D). Hence Bo is a function of other influencing parameters. Now considering the parameter relative roughness pitch (P/e), the value of $\ln \frac{100\ Nu}{(\mathrm{Re})^{0.947}\ (e/D)^{0.290}}$ has been plotted against ln (P/e) in Fig. 19. From the regression to fit

a second-order quadratic, one obtains.

$$\ln\left[\frac{100Nu}{(\mathrm{Re})^{0.947}(e/D)^{0.290}}\right] = \ln\left(2.611057415\times10^{-3}\right) + 5.885\left(\ln\left(P/e\right)\right) + \left(-1.237\left(\ln\left(P/e\right)\right)^2\right) \tag{10}$$

It can be rearranged as,

$$Nu = Co\ \ (\mathrm{Re})^{0.947}\ (e/D)^{0.290}\ (P/e)^{5.885} \times \exp^{[-1.237\ \ (\ln(P/e))^2]} \tag{11}$$

Where Co is a function of parameter representing ratio of gap position to width of absorber plate.

Finally a plot of $Nu/(\mathrm{Re})^{0.947}(e/D)^{0.290}(P/e)^{5.885} \times \exp^{\left(-1.237(\ln\ (P/e))^2\right)} = Co$ as a function of d/W, shown in Fig. 20 has been plotted. The regression analysis to fit a straight line on graph through points yields:

$$\frac{Nu}{(\mathrm{Re})^{0.947}(e/D)^{0.290}(P/e)^{5.885} \times \exp^{\left(-1.237(\ln(P/e))^2\right)}} = Do\left(d/W\right)^{0.115} \tag{12}$$

The equation can be rearranged as,

$$Nu = Do(\mathrm{Re})^{0.947}(e/D)^{0.290}(P/e)^{5.885}(d/W)^{0.115} \times \exp^{[-1.237(\ln(P/e))^2]} \tag{13}$$

The values of coefficients Ao= 0.009, Bo=0.025, Co=2.611057415×10^{-3} and Do= 3×10^{-5} are obtained from fitting the curves in Figs. 17 to 20.

The final correlation for Nusselt number can be written in the following form,

$$Nu = 3\times10^{-5}\ (\mathrm{Re})^{0.947}\ (e/D)^{0.290}\ (P/e)^{5.885}\ (d/W)^{0.115} \times \exp^{[-1.237\ (\ln(P/e))^2]} \tag{14}$$

Fig. 21 shows a comparison between the experimental values of Nusselt number and those predicted from the correlation developed in Eq. 14. Around 94% (153 out of 162) of the data points are observed to lie within $\pm$ 9%. The standard deviation is ± 4.46%. It is therefore concluded that the above heat transfer correlation is reasonably satisfactory for the prediction of the Nusselt number for the 60˚ inclined discrete wire rib roughened duct.

7. CORRELATION FOR FRICTION FACTOR

The friction factor dependents strongly on roughness parameters, e/D, P/e, d/W and the operating parameter, Re. Thus the equation for friction factor can be written as

$$f = f\left(\mathrm{Re}, e/D, P/e, d/W\right) \tag{15}$$

All the 162 numbers experimental data corresponding to 27 roughened plates are also used to develop a correlation for friction factor using regression analysis. Fig. 22 shows the friction factor as a function of Reynolds number. A regression analysis to fit a straight line on graph through the data points yields the following power law relationship between friction factor and Reynolds number.

$$f = Eo\,\mathrm{Re}^{-0.23} \tag{16}$$

The constant Eo is dependent of the parameter e/D, P/e, d/W. The relative roughness height e/D introduced to incorporate the effect of roughness height on friction factor. Now the value of $f/\mathrm{Re}^{-0.23}$ are plotted against relative roughness height of rib (e/D) as shown in Fig. 23.

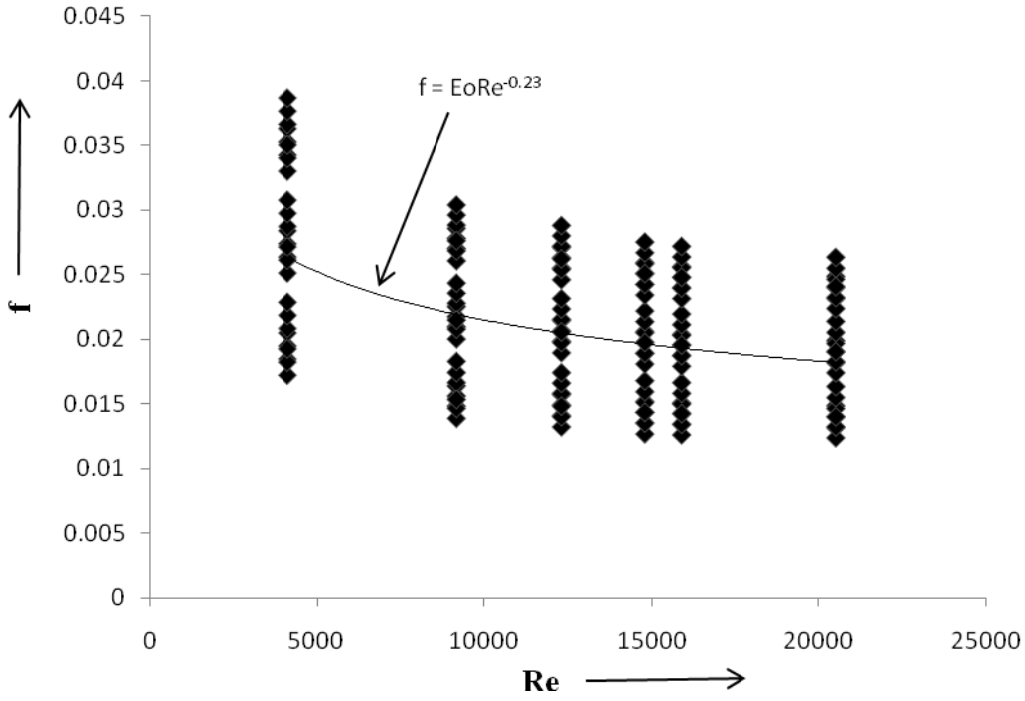

Fig. 22. Friction Factor Vs Reynolds number

The regression analysis to fit a straight line on graph through points yields:

$$f = Fo\ \mathrm{Re}^{-0.23}\left(e/D\right)^{0.804} \tag{17}$$

Such a relationship was indicated by plots of friction factor as a function of relative roughness height of rib (e/D). Hence Fo is a function of other influencing parameters. Now considering the parameter relative roughness pitch (P/e), the value of $\ln\dfrac{100f}{\mathrm{Re}^{-0.23}\left(e/D\right)^{0.804}}$ has been plotted against ln (P/e) in Fig. 24. From the regression to fit a second-order quadratic, one obtains.

$$\ln\frac{100f}{\mathrm{Re}^{-0.23}\left(e/D\right)^{0.804}} = \ln\left(1.27124917\right) + 4.516\left(\ln\left(P/e\right)\right) + \left(-0.944\left(\ln\left(P/e\right)\right)^2\right) \tag{18}$$

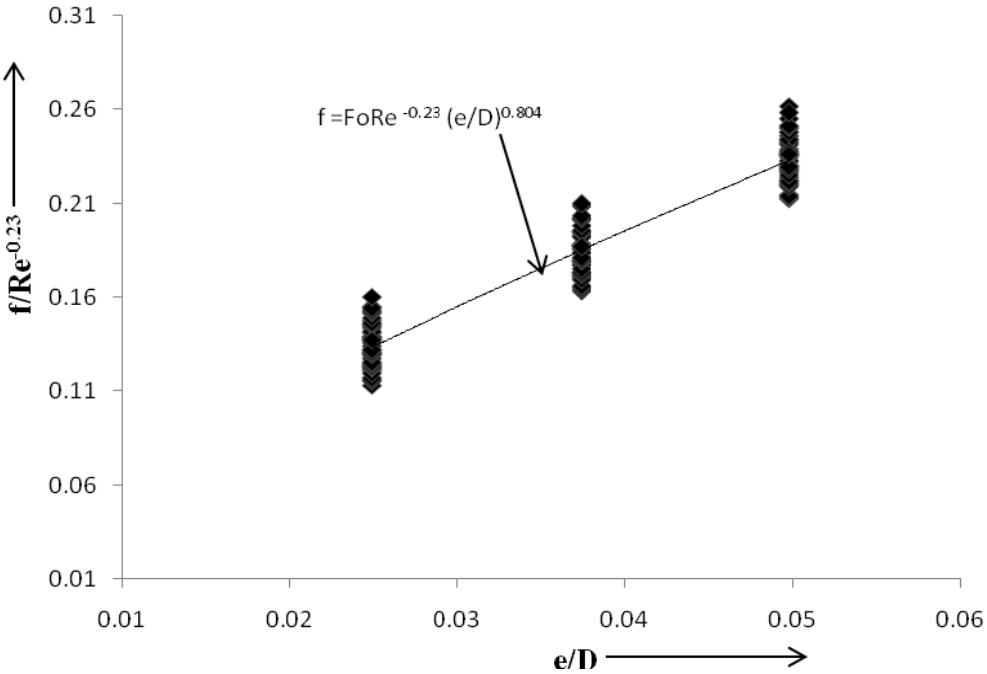

Fig. 23. $f/\mathrm{Re}^{-0.23}$ **Friction Factor Vs e/D**

It can be rearranged as,

$$f = Go\left(\mathrm{Re}\right)^{-0.23}\left(e/D\right)^{0.804}\left(P/e\right)^{4.516} \times \exp^{\left(-0.944\ \left(\ln\left(P/e\right)\right)^2\right)} \tag{19}$$

Where constant Go is a function of other remaining parameter, relative gap position of rib (d/W). This parameter is incorporated and the value of $f \Big/ \mathrm{Re}^{-0.23}\left(e/D\right)^{0.804}\left(P/e\right)^{4.516}\exp^{\left(-0.944\left(\ln\left(P/e\right)\right)^2\right)}$ are plotted against the value d/W, as shown in Fig. 25.

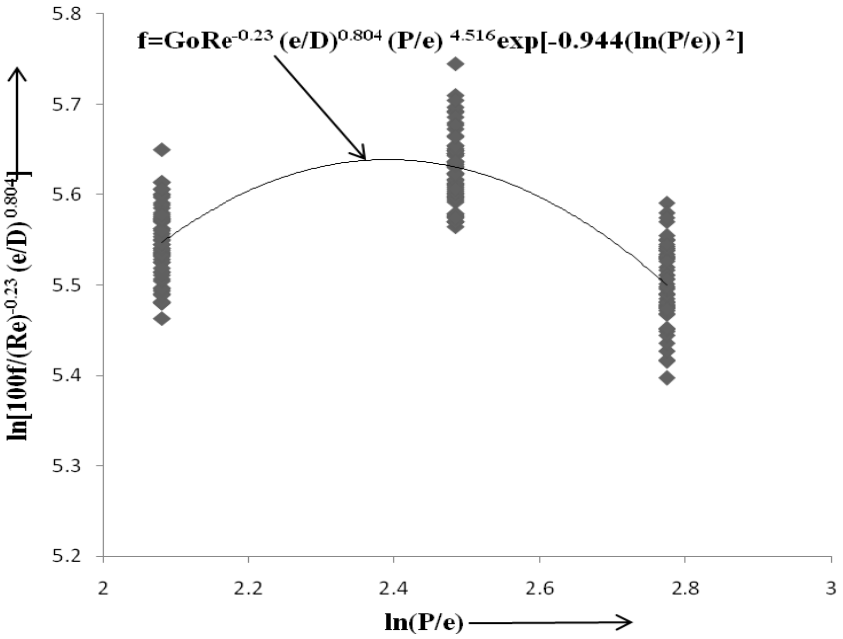

Fig. 24. $\ln \dfrac{100\,f}{\mathrm{Re}^{-0.23}\left(e/D\right)^{0.804}}$ **Vs ln (P/e)**

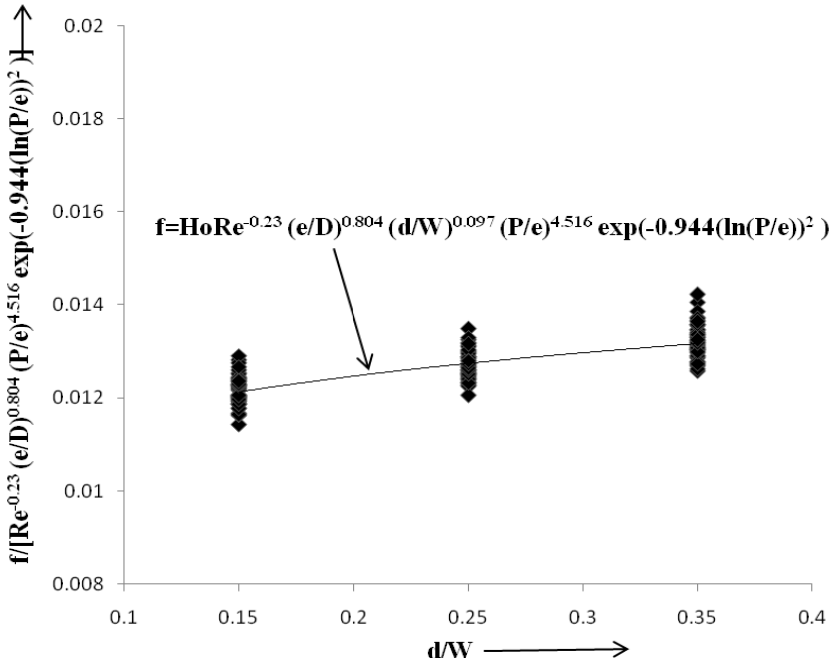

Fig. 25. $f \Big/ \mathrm{Re}^{-0.23}\left(e/D\right)^{0.804}\left(P/e\right)^{4.516}\exp^{\left(-0.944\,(\ln(P/e))^2\right)}$ **Vs d/W**

The final form of the correlation for friction factor is obtained as follows:

$$f = Ho\,\mathrm{Re}^{-0.23}\left(e/D\right)^{0.804}\left(d/W\right)^{0.097}\left(P/e\right)^{4.516}\times\exp^{\left(-0.944\left(\ln\left(P/e\right)\right)^{2}\right)} \quad (20)$$

The values of coefficients Eo= 0.180, Fo=2.601, Go=1.27124917×10^{-2} and Ho= 0.014 are obtained from fitting the curves in Figs. 22 to 25.
The final correlation for friction factor can be written in the following form,

$$f = 0.014\,\mathrm{Re}^{-0.23}\left(e/D\right)^{0.804}\left(d/W\right)^{0.097}\left(P/e\right)^{4..516}\times\exp^{\left(-0.944\left(\ln\left(P/e\right)\right)^{2}\right)} \quad (21)$$

Fig. 26 shows the comparison between the experimental values of friction factor and those predicted by the respective correlating Eq. 21. In Fig. 26, 95 % of data points lie within ± 9% (155 out of 162). The standard deviation is ±5.48%.

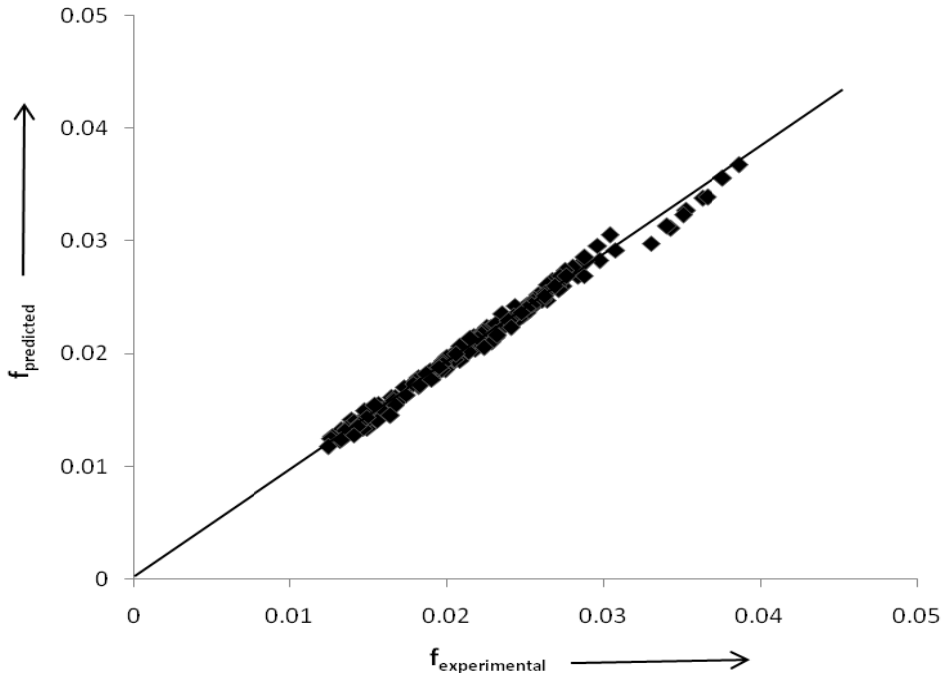

Fig. 26. Comparison of friction factor for experimental values with predicted values

8. CONCLUSIONS

Based on the experimental results of heat and fluid flow in rectangular duct with 60º inclined discrete rib roughness on one broad wall, which is subjected to uniform heat flux the main findings are:

1. As compared to smooth surface the roughened surface can yield a maximum of about 2.57-fold and 3.72-fold increase in the Nusselt number and friction factor, respectively in the range of parameter investigated.
2. The maximum heat transfer enhancement occurs for the relative roughness pitch of 12, relative gap position of 0.35 and relative roughness height of 0.0498.

3. Statistical correlations for Nusselt number and friction factor have been developed as a function of gap position, rib height (or depth), pitch and Reynolds number. These correlations have been found to predict the values of Nusselt number and friction factor with average absolute standard deviation of 3.8% and 3.4%, respectively.

REFERENCES

Bvochora, J.M., Read, J.S., Zvauya, R. (2000). Application of very high gravity technology to the cofermentation of sweet stem sorghum juice and sorghum grain. Indust. Crops Prod., 11(1), 11-17.

ASHRAE standard (1950). Methods of testing to determine the thermal performance of solar collectors. 93-77.

Bhagoria, J.S., Saini, J.S., Solanki, S.C. (2002). Heat transfer co-efficient and friction factor correlation for rectangular solar air heater duct having transverse wedge shaped rib roughness on the absorber plate. Renew. Energy, 25, 341-369.

Bhatti, M.S., Shah, R.K. (1987).Turbulent and transition convective heat transfer in ducts. W. Wiley.

Cavallero, D., Tanda, G. (2002). An experimental investigation of forced convection heat transfer in channels with rib turbulators by means of liquid crystal thermography. Exp. Thermal Fluid Sci., 26, 115-121.

Cho, H.H., Kim, Y.Y., Rhee, D.H., Lee, S.Y., Wu, S.J. (2003). The effect of gap position in discrete ribs on local heat/mass transfer in a square duct. J. Enhanced Heat Transfer, 10, 287-300.

Cho, H.H., Wu, S.J., Know, H.J. (2000). Local heat/mass transfer measurement in a rectangular duct with discrete rib. ASME J. Turbomachinery, 122, 579-586.

Gao, X., Sunden, B. (2001). Heat transfer distribution in rectangular ducts with V-shaped ribs. Heat Mass Transfer, 37, 315-320.

Gee, D.L., Webb, R.L. (1980). Forced convective heat transfer in helically rib-roughened tubes. Int. J. Heat Mass Transfer, 21, 1127-1136.

Gupta, D., Solanki, S.C., Saini, J.S. (1993). Heat and fluid flow in rectangular solar air heater ducts having transverse rib roughness on absorber plate. Solar Energy, 51, 31-37.

Han, J.C., Glicksman, L.R., Rohsenow, W.M. (1978). An investigation of heat transfer and friction for rib-roughened surfaces. Int. J. Heat Mass Transfer, 21, 1143-1156.

Han J.C., Park J.S. (1988). Developing heat transfer in rectangular channels with rib turbulators. Int. J. Heat Mass Transfer, 3, 183-195.

Han, J.C., Park, J.S., Lei, C.K. (1985). Heat transfer enhancement in channel with turbulence promoters. Trans. ASME J. Engg. Gas Turbines Power, 107, 628-635.

Han, J.C., Ou, S., Park, J.S., Lei, C.K. (1989). Augmented heat transfer in rectangular channels of narrow aspect ratios with rib turbulators. Int. J. Heat Mass Transfer, 32, 1619-1630.

Han, J.C., Zhang, Y.M. (1992). High performance heat transfer ducts with parallel, broken and V- shaped broken ribs. Int. J. Heat Mass Transfer, 35(2), 513-523.

Han, J.C., Zhang, Y.M., Lee, C.P. (1991). Augmented heat transfer in square channels with parallel, crossed, and V shaped angled ribs. Trans. ASME Journal of Heat Transfer, 113, 590-596.

Karwa, R. (2003). Experimental studies of augmented heat transfer and friction in asymmetrically heated rectangular ducts with ribs on the heated wall in transverse, inclined, V-continuous and V-discrete pattern. Int. Comm. Heat Mass Transfer, 30, 241-250.

Karwa, R., Solanki, S.C., Saini, J.S. (1999). Heat transfer coefficient and friction factor correlations for the transitional flow regimes in rib-roughened rectangular duct. Int. J. Heat Mass Transfer, 42, 1597-1615.

Karwa, R., Solanki, S.C., Saini, J.S. (2001). Thermo-hydraulic performance of solar air heaters having integral chamfered rib roughness on absorber plate. Energy, 26, 161-176.

Kays, W.M. (1966). Convective heat and mass transfer, McGraw Hill Inc., New York.

Kukreja, R.T., Lau, S.C., McMillin, R.D. (1993). Local heat/mass transfer distribution in a square channel with full and V-shaped ribs. Int. J. Heat Mass Transfer, 36, 2013-2020.

Lau, S.C., McMillin, R.D., Han, J.C. (1991). Heat transfer characteristics of turbulent flow in a square channel with angled rib. Trans. ASME J. Turbomachinery, 113, 367-374.

Lau, S.C., McMillin, R.D., Han, J.C. (1991). Turbulent heat transfer and friction in a square channel with discrete rib turbulators. Trans. ASME J. Turbomachinery, 113, 360-366.

Momin, A-M E., Saini, J.S., Solanki, S.C. (2002). Heat transfer and friction in solar air heater duct with V-shaped rib roughness on absorber plate. Int. J. Heat Mass Transfer, 45, 3383-3396.

Muluwork, K.B., Saini, J.S., Solanki, S.C. (1998). Studies on discrete rib roughened solar air heater. In: Proc. Nat. Solar Energy Convention, Roorkee, 75-84.

Prasad, B.N., Saini, J.S. (1988). Effect of artificial roughness on heat transfer and friction factor in solar air heater. Solar Energy, 41, 555-560.

Sahu, M.M., Bhagoria, J.L. (2005). Augmentation of heat transfer co-efficient by using 90˚ broken transverse rib on absorber plate of solar air heater. Renew. Energy, 30, 2057-2073.

Saini, R.P., Verma, J. (2008). Heat transfer and friction correlations for a duct having dimple shape artificial roughness for solar air heater. Energy, 33, 1277-1287.

Scott, D.F., Hewitt, A.L., MacDonald, R.A. (2002). Calibration of an orifice meter. NACA Technical Memorandum, 1940.

Sethumadhavan, R., Rao, M.R. (1983). Turbulent flow heat transfer and fluid friction in helical-wire-coil-inserted tube. Int. J. Heat Mass Transfer, 26, 1833-1845.

Tanda, C. (2004). Heat transfer in rectangular channels with transverse and V-shaped broken ribs. Int. J. Heat Mass Transfer, 47, 229 243.

Varun, Saini, R.P., Singal, S.K. (2008). Investigation on thermal performance of solar air heaters having roughness elements as a combination of inclined and transverse ribs on the absorber plate. Renew. Energy, 33, 1398-1405.

Verma, S.K., Prasad, B.N. (2000). Investigation for the optimal thermo hydraulic performance of artificially roughened solar air heaters. Renew. Energy, 20, 19-36.